# CANONICAL CEREBELLAR GRAPH WAVELETS AND THEIR APPLICATION TO FMRI ACTIVATION MAPPING

*Hamid Behjat*[1], *Nora Leonardi*[2,3], *Leif Sörnmo*[1], *Dimitri Van De Ville*[2,3]

[1] Signal Processing Group, Department of Biomedical Engineering, Lund University, SE-22100 Lund, Sweden

[2] Medical Image Processing Lab (MIPLAB), École Polytechnique Fédérale de Lausanne, CH-1015 Lausanne, Switzerland

[3] Department of Radiology and Medical Informatics, University of Geneva, CH-1211 Geneva, Switzerland

## ABSTRACT

Wavelet-based statistical parametric mapping (WSPM) is an extension of the classical approach in fMRI activation mapping that combines wavelet processing with voxel-wise statistical testing. We recently showed how WSPM, using graph wavelets tailored to the full gray-matter (GM) structure of each individual's brain, can improve brain activity detection compared to using the classical wavelets that are only suited for the Euclidian grid. However, in order to perform analysis on a subject-invariant graph, canonical graph wavelets should be designed in normalized brain space. We here introduce an approach to define a fixed template graph of the cerebellum, an essential component of the brain, using the SUIT cerebellar template. We construct a corresponding set of canonical cerebellar graph wavelets, and adopt them in the analysis of both synthetic and real data. Compared to classical SPM, WSPM using cerebellar graph wavelets shows superior type-I error control, an empirical higher sensitivity on real data, as well as the potential to capture subtle patterns of cerebellar activity.

***Index Terms***— Statistical testing, functional MRI, cerebellum, spectral graph theory, graph wavelet transform, wavelet thresholding

## 1. INTRODUCTION

In many fMRI task-evoked studies, localized brain activity can be detected by general linear model (GLM) fitting and statistical hypothesis testing. Statistical parametric mapping (SPM) is the classical method that requires Gaussian spatial smoothing of the functional data as a linear means to noise reduction [1], which comes at the cost of a loss in spatial specificity. On the other hand, wavelet methods have the power to provide an optimised representation of activation patterns through non-linear denoising. For wavelet-based statistical parametric mapping (WSPM) framework, in particular, the thresholding in the wavelet domain is considered as a denoising step only, and is followed by statistical thresholding of the reconstructed maps [2, 3].

Though WSPM using classical wavelets can circumvent SPM's drawback of a loss in specificity through wavelet processing, both SPM and WSPM assume the functional data to lie within the Euclidean space, whereas brain activity resides on a topologically complicated domain, the cerebral cortex and the cerebellar grey matter (GM). For that, we recently proposed an extension of WSPM using graph wavelets that adapt to the structure of the brain GM (sgWSPM) [4].

Although the cerebral cortex is quite similar between subjects in terms of the main fissures, there remains a significant amount of inter-subject variability in terms of the full topology. This hinders the idea of creating a high resolution full brain *template* GM graph representation from available full brain atlases such as the ICBM152 which is the most commonly used atlas and has been generated by averaging 152 anatomical scans [5], as the intricate structure of neocortex is largely lost when such a large group of subject is averaged.

However, the *cerebellum* has a unique geometry, where the whole structure as well as the number and position of its fissures are highly consistent across individuals. This fact has lead to the creation of cerebellar templates and atlases, the SUIT template being one example [6], a well established high-resolution atlas template of the human cerebellum and brain stem, defined at 1 mm cubic resolution in MNI space, which has the unique feature of being spatially unbiased; that is, the location of each cerebellar structure is equal to that of each individual within the MNI space (compare Fig. 2(a) to Fig. 3(d) as an example). The beauty of this template is that it preserves the anatomical details of the cerebellar structures and fissures through a nonlinear atlas-generation algorithm. The cerebellum is an essential component of the brain that although accounts for only 10% of the total brain weight, contains more neurons than the rest of the brain combined [7], and is responsible for monitoring and regulating motor behaviour, as well as having cognitive functions such as learning and attention.

The contribution of the current paper is twofold: first, the design of a *subject-invariant template* cerebellar graph instead of using the anatomy of individual subject cerebella; second, modification of the spectral support of a Meyer-like graph wavelet frame to construct a set of canonical cerebellar graph wavelets adapted to the template cerebellar graph. The graph is designed based on SUIT's cerebellum template [6]. Unlike our previously proposed full brain subject-variant graph design [4], the unique idea here is that the same graph template, and the corresponding wavelets, can be adopted for analysing cerebellar fMRI data in different subjects. By integrating the SUIT cerebellar template into sgWSPM, we present a new subject-invariant approach for analysing cerebellar fMRI data within the WSPM framework.

In the following, we will first give a brief recapitulation on graphs and their eigenspace (Sec. 2.1), and then describe the design of the template cerebellar graph (Sec. 2.2). We continue by reviewing the spectral graph wavelet transform (Sec. 2.3 ), describing a suitable cerebellar graph wavelet frame (Sec. 2.4), and recapping WSPM (Sect. 2.5). We present results from an application to both simulated and real cerebellar fMRI data and compare these to the standard SPM and simple univariate testing (Sec. 3).

978-1-4244-7929-0/14/$26.00 

## 2. CEREBELLAR GRAPH WAVELET-BASED ACTIVITY DETECTION

### 2.1. Weighted Graphs and Their Spectrum

Let $G = (V, E, W)$ be an undirected graph consisting of a set of $N_g$ nodes $V$, and edges $E$ with corresponding non-negative weights $W$. Assuming the graph has no loops, it can be fully defined by its adjacency matrix $A$ as

$$A_{i,j} = \begin{cases} w_{i,j} & \text{if } (i,j) \in E, \\ 0 & \text{otherwise.} \end{cases} \quad (1)$$

where $w_{i,j}$ denotes the weight of the edge between nodes $i$ and $j$. The degree matrix and normalized Laplacian matrix are given by $D_{i,i} = \sum_j A_{i,j}$ and $\mathcal{L} = I - D^{-1/2}AD^{-1/2}$, respectively. As we will see in Sec. 2.3, spectral graph wavelets are designed using the set of orthonormal Laplacian eigenvectors $\{\chi_l\}$ that satisfy $\mathcal{L}\chi_l = \lambda_l\chi_l$. The graph spectrum is defined by the corresponding set of non-negative eigenvalues $\{\lambda_l\}$.

### 2.2. Cerebellar Graph Design

We use the SUIT template and atlas as our reference in defining a cerebellar graph. The graph nodes are defined through a two-step thresholding scheme, first on the cerebellar GM probabilities of the SUIT template, followed by a second thresholding phase on the interpolated values of a downsampled version. The detailed steps are as follows:

- First, we segmented the 1mm cubic resolution SUIT cerebellar template (Fig. 2(a)) to extract the GM, suitGM (Fig. 2(b)), using the unified segmentation algorithm [8] that leads to a probability map indicating the probability of each voxels being GM, white matter (WM), or cerebrospinal fluid (CSF). Next, we thresholded suitGM and only kept voxels for which the GM probability was higher than that of WM or CSF, resulting in mask G1.
- Second, in order to remove the brain stem and only keep the cerebellar structure in a non-subjective way, we made use of SUIT's probabilistic atlas of the 34 cerebellar lobules [9], and masked out any voxel that did not lie within this atlas. Moreover, minute isolated regions that resulted from the segmentation phase were also removed to achieve a single connected mask G2. We denote the GM probability of each voxel $i$ within suitGM by $v_i$, and its membership with respect to G2 by a logical variable $\mathrm{v}_i$.
- Next, we created a symmetric downsampled version of G2 using a nearest neighbour interpolation scheme combined with the second thresholding step as

$$v_n^d = \begin{cases} \frac{1}{N^3}\sum_{m=1}^{N^3} \mathrm{v}_m v_m & \text{if } \frac{1}{N^3}\sum_{m=1}^{N^3} \mathrm{v}_m v_m \geq 0.5, \\ 0 & \text{otherwise} \end{cases} \quad (2)$$

  where $N$ denotes the downsampling factor, $m$ runs over the local neighbourhood voxels within the high resolution volume, $v_n^d$ is the GM probability of the $nth$ downsampled voxel. We denote the resulting mask with G, and treat the remaining voxels within G as graph nodes.

  A downsampled version of G2 was required due to its incomparable and unnecessary high 1 mm cubic MNI resolution compared to that of typical functional data ($2-3$ mm cubic). Also, instead of initially downsampling the SUIT template and proceeding with constructing the mask, we found it beneficial to first make use of the finer anatomical detail within the original high resolution SUIT template; that is, we derived the mask based on the more accurate GM probabilities and then did a linear downsampling within the MNI space in the final stage, leading to a more accurate downsampled GM mask and GM probabilities.

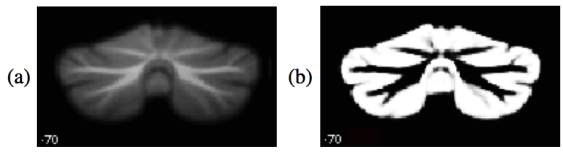


**Fig. 2:** An image of a coronal slice of (a) SUIT cerebellum template and (b) the corresponding extracted GM.

- Finally, we created a weighted graph by computing the three-dimensional connections between adjacent voxels in G based on the 26-connected neighborhood. The weight of the edge between vertices $i$ and $j$ was defined as $w_{i,j} = (P_iP_j)^5$, where $P_i$ and $P_j$ correspond to the GM probability of the vertices $i$ and $j$, respectively. This weighting is empirical and heavily penalizes connections between vertices with low GM probability, and enhances the diffusion of the wavelets along regions of GM with high probability [4]. We also created a binary graph version, by binarizing the remaining voxels in G, and only computing the connections.

### 2.3. Spectral Graph Wavelet Transform

We give a short overview of spectral graph wavelets and refer to [10] for further details. Classical wavelets are formed through shifting and scaling of a mother wavelet $\psi$ within the Euclidian space. However, constructing wavelets that diffuse on arbitrary domains such as graphs is not straightforward, for which [10] has appealed to the Fourier domain. The Fourier transform of the classical continuos wavelet $\psi_{s,a}(x) = \frac{1}{s}\psi\left(\frac{x-a}{s}\right)$, at scale $s$ and location $a$, is given by $\psi_{s,a}(x) = \frac{1}{2\pi}\int_{-\infty}^{\infty}\hat{\psi}(s\omega)e^{-j\omega a}e^{j\omega x}d\omega$. We see that scaling $\psi$ by $1/s$ corresponds to scaling $\hat{\psi}$ by $s$, and the wavelets can be interoperated as scaled bandpass filters.

By observing that the complex exponentials, $e^{jwx}$, are the basis functions of the Fourier transform, and are themselves eigenvectors of the 1-D Laplacian operator, we can in analogy, interpret the the eigenvectors of the graph Laplacian as defining the graph *spectrum*, the analogue of the Fourier domain of signals within Euclidian space [11]. Thus, the graph Fourier transform of a graph signal $f$ is given by $\hat{f} = \langle f|\chi_\ell\rangle$, where $\langle\ |\ \rangle$ denotes the inner product. The spectral graph wavelets at $J$ scales localized on each graph node $n$ are then obtained as

$$\psi_{j,n}(m) = \sum_{l=0}^{N_g-1} g(t_j\lambda_l)\chi_l^*(n)\chi_l(m), \quad j = 1,\dots J, \quad (3)$$

where $t_j$ denotes the wavelet scale. The corresponding wavelet coefficients are given by $\mathrm{w}_\psi(j,n) = \langle\psi_{j,n}|f\rangle$. A scaling function which captures the lowpass components can also be defined using a suitable kernel $\phi$ in a similar fashion.

### 2.4. Wavelet Frame Adapted to the Cerebellum

We used the normalized graph Laplacian matrix $\mathcal{L}$, for which the spectrum is confined to eigenvalues in the range [0,2), and a modified version of the Meyer-like tight frame design, which conserves energy in the wavelet domain [12]. By empirical testing, we found

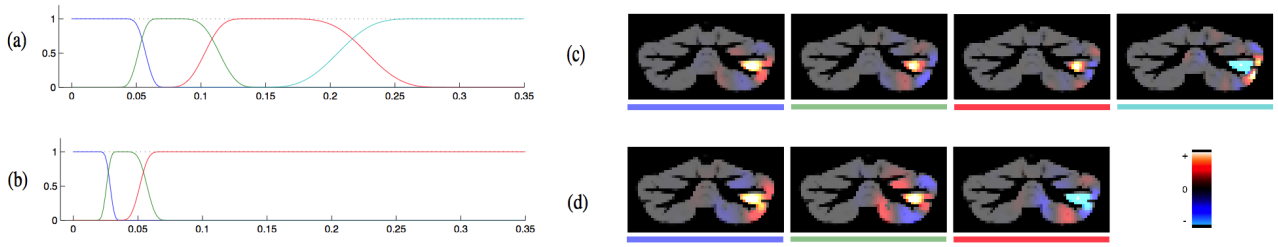


**Fig. 1:** Meyer-like windowing functions $g(t_j\lambda)$ at the lower end of the graph spectrum and a realisation of their corresponding wavelets overlaid on the segmented GM of the SUIT template. Scaling function and wavelet supports as used (a) in [4] for *full brain* graphs, and (b) that used for the proposed template *cerebellar* graph. (c)-(d) An illustration of the cerebellar wavelets corresponding to the windowing functions in (a) and (b), respectively (color-coded). Note that the wavelets diffuse within 3 dimensional space but we here only illustrate an image of a coronal slice.

that the finest scales of the graph wavelets did not significantly contribute to detection performance, and therefore, we adapted the windowing functions by adjusting the scaling parameter $t_j$. Compared to our previous wavelet frame adapted to single subject full brain [4] (see Fig. 1(a)), the spectral support of the scaling function and first wavelet kernel was confined by a factor of about 2 (see Fig. 1(b)). This is an interesting observation and can be linked to the lower extent of geometrical detail of the cerebellum template compared to that of the domain defined by the GM of the full brain, which includes the convoluted structure of the cerebral cortex.

Figs. 1(c)-(d) depict a realisation of the scaling function and wavelets in the spatial domain, overlaid on suitGM. We observe that for both the scaling function and wavelets, the scale of the kernels in Figs. 1(d) is coarser than the ones in Figs. 1(c), which is in accordance with the definition of the windowing functions.

Also, we notice the difference in the size of the cerebellar graph compared to that of a full brain one (15 k vs more than 40 k), which in itself can effect spectral properties. The main challenge is to design wavelet frames that adapt to a graphs structure, or in other words, its spectrum; however, a second inherent challenge is the estimation and study of the full spectrum of such large graphs, which is computationally restrictive.

### 2.5. Wavelet-Based SPM

We give a brief overview of the WSPM framework and refer to [2, 3] for details. In single-subject WSPM, a wavelet transform is computed for each functional volume and a GLM is fitted to the time evolution of each wavelet coefficient, whereas within the normal SPM the model fitting is done on the temporal behaviour of the voxels themselves. Using the estimated effect sizes and residual errors, wavelet domain $t$-values are constructed and then thresholded. The wavelet domain thresholding (by $\tau_w$) is considered as a denoising step only, and is followed by spatial domain statistical thresholding (by $\tau_s$) of the reconstructed maps such that the null-hypothesis rejection probability is properly controlled; the optimal combination of $\tau_w$ and $\tau_s$ is calculated by minimizing the worst-case error between the unprocessed and the detected parameter map [2]. Using the inverse wavelet transform the reconstructed *processed* parameter map after bias reduction, $\tilde{\mathbf{u}}$, is computed as

$$\tilde{\mathbf{u}} = \min\left(\sum_k \mathbf{u}[k]\boldsymbol{\psi}_k, \sum_k H(|\mathbf{t}[k]| - \tau_w)\mathbf{u}[k]\boldsymbol{\psi}_k\right) \quad (4)$$

where the index $k$ runs over all scales of the decomposition and the functions $\psi_k$ corresponds to the associated scaled, shifted, and dilated versions of the scaling function or of the wavelet, $\mathbf{u}$ are the wavelet coefficients, $\mathbf{t}$ are the wavelet domain $t$-values and $H$ is the Heaviside step function [2]. Finally, by thresholding the constructed spatial domain t-values by $\tau_s$, the final parameter map of detected activations can be computed as $\bar{\mathbf{u}} = H\left(\frac{\tilde{\mathbf{u}}}{\sum_k \boldsymbol{\sigma}[k]|\boldsymbol{\psi}_k|} - \tau_s\right)\tilde{\mathbf{u}}$, where $\boldsymbol{\sigma}$ is the standard deviations of the error estimates.

## 3. EXPERIMENTAL RESULTS

### 3.1. Synthetic Data

A synthetic cerebellar dataset was created in a way similar to that in [4] but here using the SUIT template instead of an individual subject's anatomical scan, see Fig. 3(a). Table 1 summarizes the activation mapping performance using simple univariate testing (no smoothing), SPM (isotropic Gaussian smoothing, FWHM = 6 mm) and sgWSPM (no smoothing). For sgWSPM, we present results using three different settings. SPM shows the highest sensitivity. This is expected due to the initial smoothing phase, but comes at the cost of detecting a large number of false positives (type-I error), see Fig. 3(b). On the other hand, sgWSPM on the non-smoothed data using spectral support design as in Fig. 1(b), leads to a high sensitivity with well-controlled specificity resulting in detected patterns unvailing the fine detail structure of the ground truth activity such as that in the right superior region, see Fig. 3(c). Compared to simple univariate testing, where we use the original non-smoothed data as in the wavelet approach but without nonlinear wavelet denoising, we see the strength of the wavelet framework in taking into account spatial correlations. Although the weighted approach leads a slightly pronounced sensitivity (86.4 vs 83.2) with a small 0.6% drop in specificity, this enhancement is less significant as that observed for the single subject full brain graph [4] (results not shown). This is due to the fact that there is more certainty in the GM probabilities in the SUIT atlas as to that of the full brain, and thus the effect of weighting the edges becomes less pronounced as the adjacency matrix is closer to the binary one.

| Method | uni-variate | SPM | sgWSPM | | |
|---|---|---|---|---|---|
| | | | Fig. 1a | Fig. 1b | |
| | | | binary | | weighted |
| Detections | 88 | 5714 | 2704 | 3386 | 3564 |
| Sensitivity (%) | 2.5 | 93.4 | 70.2 | 83.2 | 86.4 |
| Specificity (%) | 100 | 78 | 97.5 | 95.5 | 94.9 |

**Table 1:** Summary of the results obtained by simple univariate testing, SPM, and sgWSPM for the synthetic data set. sgWSPM results are presented for both wavelet spectral support options as in Fig. 1, and also the weighted graph option for the latter design (i.e, Fig. 1b) .

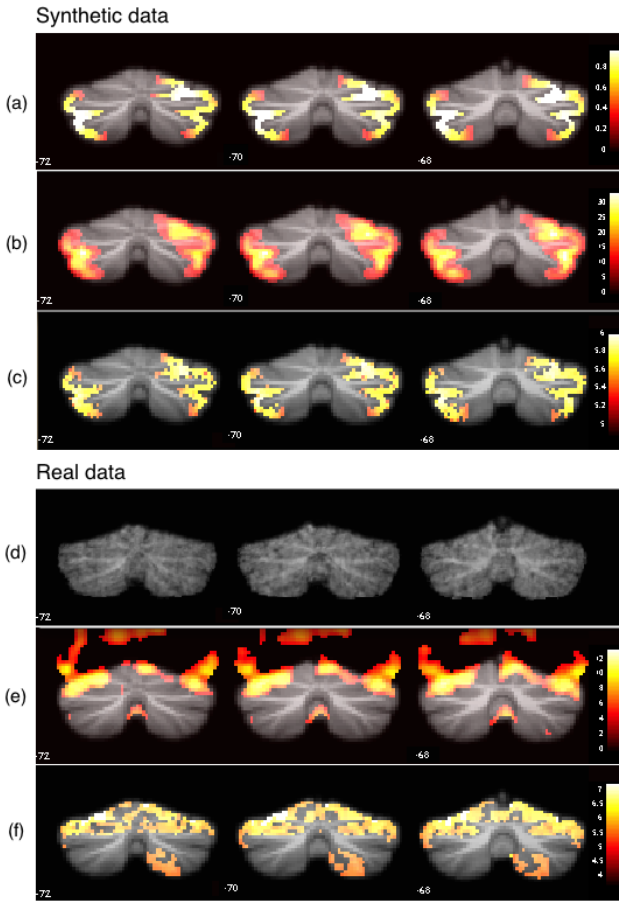


**Fig. 3:** (a) Ground truth for synthetic dataset. Detected parameter maps using (b) SPM and (c) sgWSPM. Real dataset - (d) subject's cerebellum aligned to SUIT space, detected parameter maps using (e) SPM, and (f) sgWSPM. All parameters maps thresholded for a $p < 0.05$ FWE corrected, and overlaid on SUIT template.

### 3.2. Real Data

We used a single subject data from a dataset acquired on a 3T Siemens Allegra scanner while subjects performed an event-related Eriksen Flanker task [13]. The task consisted of indicating the direction of a central arrow, which was surrounded by arrows of the same (congruent) or opposite direction (incongruent trial). Note that using the proposed template cerebellar graph, we are required to normalize the functional data to the SUIT space, by first extracting and mapping the subject's cerebellum into SUIT space, and using the resulting transformation to map the functional data.

Figs. 3(e)-(f) show the activations during incongruent trials detected by SPM (isotropic Gaussian smoothing, FWHM $=$ 6 mm) and sgWSPM, respectively (binary graph, with wavelet supports as in Fig. 1(b)). As in the synthetic case, SPM shows smooth maps, but in this case we also observe that the detected maps within the cerebellum leak into higher cerebral regions of the visual cortex and vice versa. We did not mask out these detections, to show the effect of the pre-smoothing required for SPM. On the other hand, in contrary to the synthetic dataset, sgWSPM shows a higher empirical sensitivity, as evidenced not only within the superior cerebellar structures but also the additional structure detected within the right inferior region. Moreover, sgWSPM maps show greater geometrical detail. The total number of detections using SPM and sgWSPM is 10486 and 6171, respectively, where only 6524 of SPM detections lie within the defined region by SUIT template, and only 3534 overlap with cerebellar GM of probability greater than $50\%$. Empirically, detections outside the latter region are most likely false positives as the BOLD signal is only expected within GM [14].

## 4. CONCLUSION

We have further extended the framework of anatomically-adapted wavelets for fMRI statistical analysis by constructing a template cerebellar graph and designing canonical cerebellar graph wavelets. The cerebellum is well suited for this approach due to its limited inter-subject variability. Compared to conventional SPM analysis, the application of the cerebellar wavelets within the WSPM framework showed superior performance in terms of type-I error control and sensitivity to detect subtle activity patterns, both for synthetic and real data. Our results suggest that the proposed cerebellar graph and wavelets can now be exploited to fMRI analysis at the group level, either for the cerebellum alone or the whole brain, in the near future.

## 5. ACKNOWLEDGEMENTS

This work was supported in part by the Swedish Research Council under grant #2009-4584 and in part by the Swiss National Science Foundation under grant PP00P2-146318.

## 6. REFERENCES

[1] K. J. Friston, A. P. Holmes, K. J. Worsley, J.-P. Poline, C. D. Frith, and R. S. J. Frackowiak, "Statistical parametric maps in functional imaging: a general linear approach," *Hum Brain Mapp*, vol. 2, pp. 189–210, 1994.

[2] D. Van De Ville, T. Blu, and M. Unser, "Integrated wavelet processing and spatial statistical testing of fmri data," *Neuroimage*, vol. 23, pp. 1472–1485, 2004.

[3] D. Van De Ville, M.L. Seghier, F. Lazeyras, T. Blu, and M. Unser, "WSPM: wavelet-based statistical parametric mapping," *Neuroimage*, vol. 37, pp. 1205–1217, 2007.

[4] H. Behjat, N. Leonardi, and D. Van De Ville, "Statistical parametric mapping of functional mri data using wavelets adapted to the cerebral cortex," in *Proc. Int. Symp. Biomed. Imaging*, 2013, pp. 1070–1073.

[5] A. C. Evans, D. L. Collins, S. R. Mills, E. D. Brown, R. L. Kelly, and T. M. Peters, "3d statistical neuroanatomical models from 305 mri volumes," in *IEEE Nuclear Science Symp. & Med. Imaging Conf.*, 1994, pp. 1813–1817.

[6] J. Diedrichsen, "A spatially unbiased atlas template of the human cerebellum," *NeuroImage*, vol. 33, no. 1, pp. 127–138, 2006.

[7] G. M. Sheperd, *The Synaptic Organization of the Brain.*, Oxford University Press, New York, 1974.

[8] J. Ashburner and K. J. Friston, "Unified segmentation," *NeuroImage*, vol. 26, no. 3, pp. 839–851, 2005.

[9] J. Diedrichsen, J. H. Balsters, J. Flavell, E. Cussans, and N. Ramnani, "A probabilistic mr atlas of the human cerebellum," *NeuroImage*, vol. 46, no. 1, pp. 39–46, 2009.

[10] D.K. Hammond, P. Vandergheynst, and R. Gribonval, "Wavelets on graphs via spectral graph theory," *Appl. Comput. Harmon. Anal.*, vol. 30, pp. 129–150, 2011.

[11] F.R.K. Chung, *Spectral graph theory*, AMS, Providence, RI, 1997.

[12] N. Leonardi and D. Van De Ville, "Tight wavelet frames on multislice graphs," *IEEE Trans. on Signal Proc.*, vol. 61, no. 13, pp. 3357–3367, 2013.

[13] A. M. Clare Kelly, L. Q. Uddin, B. B. Biswal, F. X. Castellanos, and M. P. Milham, "Competition between functional brain networks mediates behavioral variability," *NeuroImage*, vol. 39, no. 1, pp. 527–537, 2008.

[14] N.K. Logothetis and B.A. Wandell, "Interpreting the bold signal," *Ann. Rev. Physiol.*, vol. 66, pp. 735–769, 2004.